The Impact of Linear and Nonlinear Control Structures on the Performance of a Wave Energy Converter

Carrie M. Hall
Mechanical, Materials, and Aerospace Engineering Department, Illinois Institute of Technology
Chicago, Illinois, USA

Yueqi Wu, Wanan Sheng and George Aggidis
Energy Engineering Department, Lancaster University
Lancaster, United Kingdom

Optimal control techniques can oversee the power take-off (PTO) operation of wave energy converters to ensure that the overall power output is maximized, but optimization in real time poses difficulties given the wave variability and the underlying constraints of the system. This study examines model predictive control approaches that utilize a model of the hydrodynamics of the wave energy converter and the dynamics of a hydraulic PTO system. The impact of leveraging linear and nonlinear models of the dynamics in the optimization and the role of constraints on the wave energy converter performance are explored for irregular wave conditions.

KEY WORDS: Wave energy conversion, power take-off control, optimal control, model predictive control, constraints.

INTRODUCTION

As global energy demands and climate concerns continue to grow, the need for a broader range of renewable energy options is becoming increasingly clear. Although wave energy converters (WECs) have been researched for decades, much work has focused on the design of such systems. Many different structures have emerged over the years, including point absorbers, attenuators, oscillating water columns, and reservoirs (Aderinto and Li, 2018). The maximum energy will be captured if the frequency of the WEC system matches the dominant frequency of the incoming wave (i.e., resonance), and this is typically achieved by a power take-off (PTO) operation system that can effectively add or remove damping and thereby affect the device's frequency. A wide range of PTO systems exist, including turbines, hydraulic systems, and linear actuators (Têtu, 2017).

Controlling the PTO system remains challenging because of the growing complexity of WEC systems and the variable nature of the incoming waves. Early strategies often manipulated the PTO system by leveraging linear models and velocity tracking, complex conjugate approaches, or impedance matching control. Studies such as those of Hals et al. (2011a) and García-Violini et al. (2020) have compared a variety of these techniques. Although these methods have merits, they often encounter challenges with operation over a wide frequency range and at times suffer from a high computational burden. Those with feedforward components also need a wave excitation estimation and, as such, are more prone to performance problems due to wave prediction errors (García-Violini et al., 2020).

In recent years, optimization approaches have been more heavily used. Because the aim is to maximize energy production, a wide variety of optimal control strategies have been explored, including model predictive control (MPC) (Hals et al., 2011b; Li and Belmont, 2014), spectral and pseudospectral methods (Genest and Ringwood, 2016; Garcia-Violini and Ringwood, 2021), flatness-based strategies (Li, 2017), and moment-based approaches (Faedo et al., 2018). A more complete view of the evolution of WEC control approaches is available in Ringwood (2020). MPC is a natural choice for WECs but has three primary challenges: (1) the need for an accurate WEC model, (2) the need for an estimate of future wave forces, and (3) a requirement to solve for solutions with at times conflicting constraints. This study focuses on the first and third challenges.

A WEC is a complex hydrodynamic system with nonlinear dynamics. As such, creating a control-oriented model for a WEC system is not trivial. Whereas most of the existing control efforts have leveraged linear models, linearity is typically a poor assumption for a controlled WEC system, because large motions can be induced that take the system far from the equilibrium point about which it was linearized (Penalba and Ringwood, 2019; Windt et al., 2021). Using a nonlinear model enables better results, but nonlinear optimization can be computationally intensive. Given the challenges with capturing WEC dynamics in a control-oriented model, some efforts have also explored model-free approaches such as extremum-seeking control (Garcia-Rosa et al., 2012; Sun et al., 2018; Pasta et al., 2021).

For real-life applications, the MPC will need to work in real time with predictions and also ensure that the control actions do not violate any constraints. If constraints are ignored, control becomes more straightforward and leads to approaches such as the complex-conjugate control or impedance-matching control strategies. Although these approaches can have high theoretical power outputs, they often require large motions, forces, and power changes that cannot practically be

achieved (Faedo et al., 2017). In reality, PTO systems will have constraints on their motion and the maximum force they can generate for both reactive and damping actions. Constraints are typically placed on the position or velocity of the WEC mass (Hals et al., 2011b; Fusco and Ringwood, 2013), but studies have also added constraints on variables related to the control input and rate of change of the control input for a generic PTO (Li and Belmont, 2014; Richter et al., 2014; Cavaglieri et al., 2015; Zhan et al., 2020; Previsic et al., 2021; Zhang and Li, 2022), direct drive PTO (Brekken, 2011; Amann et al., 2014; Haider et al., 2021), rotary PTO (Bracco et al., 2020; Sergiienko et al., 2021), linear permanent magnet generator PTO (Jama et al., 2014; O'Sullivan and Lightbody, 2017), and hydraulic PTO (Hendrikx et al., 2017). In many such studies, the dynamics of the PTO are not included, which simplifies the solution but may result in solutions that require control responses that are not achievable as a result of the PTO's time delay.

Limits on maximum PTO power have also been introduced but are less common in part because they make the solution more difficult (Faedo et al., 2017). Even including both force and displacement constraints can be challenging because at high excitation levels, it may be impossible to abide by all constraints (Bacelli and Ringwood, 2013; Ringwood, 2020). Iterations that have included PTO power constraints have also included constraints on the electric motor (Kovaltchouk et al., 2015; Sergiienko et al., 2022), as well as power flow and force constraints for a hydraulic PTO (Karthikeyan et al., 2019). Efforts that have introduced constraints with PTO dynamics typically attempt to capture the dynamics via a simple loss term (Bacelli et al., 2015; Karthikeyan et al., 2019; Mérigaud and Tona, 2020). This is a step toward a more realistic solution but may still oversimplify the situation.

As devices aim to capture more energy, they are becoming increasingly complex, which brings potentially more constraints into the system. One such device is the TALOS WEC, which is studied in this paper and shown in Fig. 1. TALOS is a multi-degree-of-freedom (DOF) point-absorber style WEC with an outer hall that contains a mass linked to the hull via hydraulic cylinders (Aggidis and Taylor, 2017). Several multi-DOF WECs have been developed over the years, including Pelamis (Parker et al., 2007) and TALOS, and these have the potential to harness a greater amount of wave energy. With the inertial mass PTO of TALOS, the motion of the main mass drives hydraulic fluid through the circuit. Although initial studies have demonstrated that this design may be a promising method of capturing energy from multiple directions, its enclosure in an exterior hull places strict constraints on the limits of the motion of the mass, and as such, the constraints considered in this paper will be critical for application to TALOS.

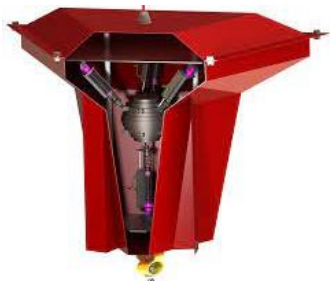

Fig. 1 TALOS WEC

Past studies have examined a variety of WEC configurations and control structures, but the influence of underlying control structure and constraints for a WEC design that has strict physical motion limitations similar to those encountered on the TALOS WEC have not been fully explored. The constraints that the design of TALOS places on the PTO may limit its effectiveness, but a predictive control may help overcome these limitations. Predictive control may present more of a benefit on TALOS than simpler WEC designs as a result of the need to abide by more constraints, and this study seeks to quantify that impact and identify control structures that are most suitable for constrained, enclosed WEC systems such as TALOS. This paper examines several different MPC structures with PTO position and power constraints in conjunction with a nonlinear hydrodynamic model and a nonlinear PTO model. The impact of using linear versus nonlinear models with by the MPC and the impact of constraints will be assessed, and the computational burden and accuracy of several approaches will be contrasted.

MODEL AND CONTROL STRUCTURE

Over the years, many different WEC designs have been investigated. This study focuses on a point absorber WEC that utilizes a hydraulic PTO. Because the primary focus is on understanding the impact of model selection and constraints on the control, a simple one-dimensional (1D) case is considered. A hydraulic PTO system is used because they are cost effective and rely on established technology. The results will be used to guide development of a three-dimensional PTO control system in future work.

WEC Model

The model and constraints are based on the TALOS WEC shown in Fig. 1. In the TALOS device, the relative motion between the hull and central mass drive fluid through the hydraulic circuit. Because the aim of this paper is to investigate control structures that are suitable for the device, control methods are tested with a simplified model at this stage. This model focuses on the motion of the central mass in the heave direction because this has been found to be one of the degrees of freedom containing the most energy for capture. Future work will examine motion in the pitch and surge directions, as these also have high amounts of energy. The motion of the central mass in TALOS is constrained by the hull and PTO elements, and these constraints will be accounted for in the control approach. The basic structure of the simplified system is shown in Fig. 2, in which there is a main mass (M) and the WEC aims to harness motion in the heave direction. The axis system used assumes an incident wave in the surge direction (x) with the wave motion in the heave direction (z) being harnessed by the WEC.

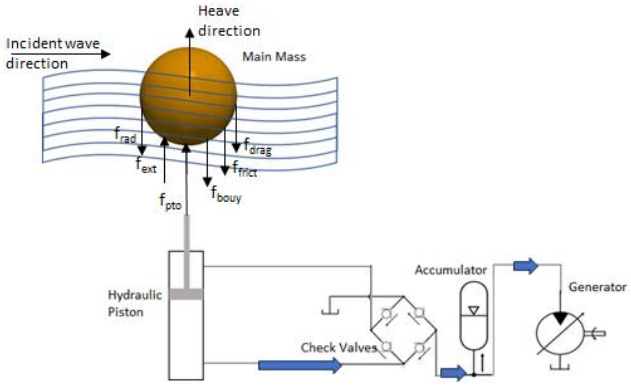

Fig. 2 Point absorber WEC system with hydraulic PTO

As the mass moves up and down with the wave, it will pump hydraulic fluid through a circuit driving a generator. To maximize the energy capture, the PTO system settings can be adjusted to apply a varying force on the hydraulic piston. The aim of the control system is to decide on the PTO force that will maximize the generator power output. Although the figure only shows one hydraulic piston as illustrated in Fig. 1, a piston could be located above and below the main mass, and

as such, forces could act in both positive and negative directions. The hydrodynamic model predicts the velocity of the main mass that is translated to the piston, and the PTO model captures the damping force supplied based on the velocity and underlying PTO dynamics as in Bacelli et al. (2008).

The hydrodynamics of the point absorber are modeled using potential flow theory to compute the hydrodynamic forces. Applying Newton's second law to the absorber, the forces acting on the body include the forces as a result of radiation (f_{rad}), restoring force (f_{res}), drag (f_{drag}), and the wave excitation force (f_{ext}), together with the force generated by the PTO (f_{PTO}). Additional forces may be present such as a mooring force or tidal force, but these are excluded here. Nonlinear forces including the nonlinear free surface effect and low frequency wave drift force are not considered. As such, the dynamics of the point absorber under the above forces are given as follows for the absorber mass *M* and position *z*:

$$(M + m_\infty)\ddot{z}(t) = -f_{\text{rad}} - f_{\text{res}} - f_{\text{drag}} + f_{\text{ext}} + f_{\text{PTO}}. \quad (1)$$

where *z* is the heave motion of the point absorber, *M* the absorber mass, and m_∞ the added mass at infinite frequency. The PTO force acting on the point absorber was computed via the PTO submodel and MPC control action. Here, an irregular wave with a significant wave height of 5 m and peak period of 10 s for a Bretschneider spectrum was created with a 0.05 s resolution; see the wave elevation time series in Fig. 3.

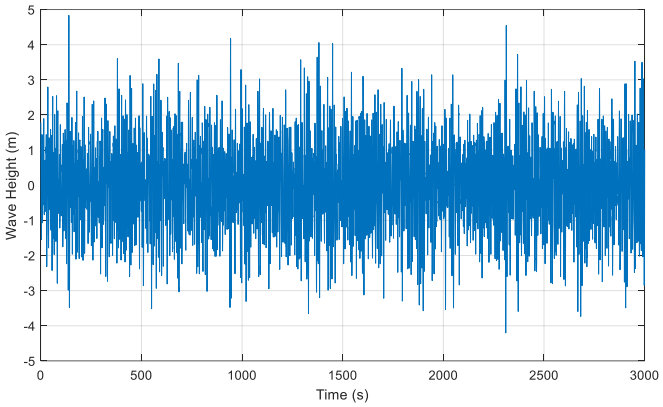

Fig. 3 Wave height profile

The added mass at infinite frequency, m_∞, is assessed via WAMIT F2T (frequency to time domain transform) for the TALOS device with the shape illustrated in Fig. 1. The radiation force in time domain (i.e., the memory effect) can be approximated using either the Prony approximation (see details in Sheng et al., 2022) or a set of first-order differential equations (Duarte et al., 2013), expressed in a state space as

$$f_{\text{rad}} = \boldsymbol{C_r q} \quad (2)$$

where

$$\dot{\boldsymbol{q}} = \boldsymbol{A_r q} + \boldsymbol{B_r}\dot{\boldsymbol{z}} \quad (3)$$

in which $\boldsymbol{q}$ is the radiation auxiliary state vector, and $\boldsymbol{A_r}$, $\boldsymbol{B_r}$, and $\boldsymbol{C_r}$ are the radiation state matrices. For the TALOS device, the appropriate $\boldsymbol{A_r}$, $\boldsymbol{B_r}$, and $\boldsymbol{C_r}$ matrices were computed using the WAMIT results for TALOS along with the *SS_Fitting* preprocessing module developed by NREL along with MATLAB's Frequency Domain Identification (FDI) toolbox.

The restoring force is given by

$$f_{\text{res}} = \rho g A_w z \quad (4)$$

in which ρ is the density of water, g is the gravitational acceleration, and A_w is the sectional area of the water plane (in the *z* direction).

The drag relationship is expressed in Eq. 5 as a quadratic function of the difference between the velocity of the central mass and the velocity of the water surface (v_f) and is dependent on the submerged surface of the WEC (A_w) and the viscous drag coefficient (C_d). The drag coefficient was taken as 3.5 based on the drag coefficients found in studies by Brown (2017) and Quartier et al. (2021) for similarly shaped devices. The overall model performance was compared with a more detailed TALOS model to validate.

$$f_{\text{drag}} = \frac{1}{2}\rho A_w C_d \left|\dot{z} - v_f\right|\left(\dot{z} - v_f\right) \quad (5)$$

Hydraulic PTO Model

The hydraulic PTO model is based on a previously developed state-space model (Bacelli et al., 2008) that has been leveraged extensively for WEC PTO control studies, although typically decoupled from the hydrodynamics. As illustrated in Fig. 2, this model includes four check valves that rectify the alternating flow of the hydraulic fluid from the piston-cylinder assembly. A gas accumulator is included to smooth the flow, and the final fluid flow drives a hydraulic motor producing power output. The model includes losses associated with the pressure drops in the pipes, motor leakage, and friction. The PTO model establishes the links between the torque output of the generator and the damping force the PTO produces and applies to the cylinder. These dynamics are often neglected in control evaluation, and a direct link between the PTO force and power output is assumed. However, in a hydraulic PTO system, this may be a poor assumption given the anticipated delay in the dynamics.

The full PTO model derivation is detailed in Bacelli et al. (2008) and results in two nonlinear differential equations that summarize the PTO dynamics. The first equation captures the dynamics of the accumulator volume (*V*) by

$$\dot{V} = -k_l \cdot P_a(V) - \frac{D}{J} \cdot L + S \cdot \dot{z} \quad (7)$$

in which k_l is a motor leakage coefficient, $P_a(V)$ is the accumulator pressure posed as a function of *V*, *D* is the motor constant, *J* is the inertia momentum of the hydraulic motor shaft, *L* is the hydraulic motor shaft angular momentum, *S* the piston cross-sectional area, and $\dot{z}$ is the piston velocity. An isentropic model of the accumulator pressure (P_a) is used with the form

$$P_a(V) = \frac{P_{\text{pr}}}{\left(1 - \frac{V}{V_a}\right)^{\kappa}} \quad (8)$$

where P_{pr} is the pre-charge pressure, V_a is the accumulator volume, and κ is the specific heat ratio.

The dynamics of the motor shaft angular momentum (*L*) are expressed in a second differential equation for the PTO as

$$\dot{L} = D \cdot \eta_m \cdot P_a(V) - \frac{B}{J} \cdot L - T \quad (9)$$

in which η_m is the motor efficiency, *B* is the motor friction, and *T* is the generator torque. With this dynamic model, the PTO force can be related to these dynamics via

$$f_{\text{PTO}} = S \cdot P_a(V) + S \cdot k(S \cdot \dot{z}) \quad (10)$$

where $k(S \cdot \dot{z})$ captures the pressure loss in a pipe due to friction under laminar conditions via the Haaland approximation of the Darcy equation, given in the equation below.

$$k(S\cdot\dot{x}) = \frac{K_s\cdot(L_g+L_{\text{eq}})\cdot\rho_{hf}\cdot S\cdot\dot{z}}{2Re\cdot D_h\cdot A^2}|S\cdot\dot{z}| \quad (11)$$

K_s, L_g, L_{eq}, and D_h are the pipe cross-section shape factor, geometric pipe length, equivalent length of local resistance, and hydraulic diameter of the pipe, respectively. The term ρ_{hf} represents the density of the hydraulic fluid, and A is the pipe cross-sectional area.

Combining all the aforementioned together, the system can be described by six first-order equations in a representation known as a state space model. Such a model captures the relationship between inputs, outputs, and variables known as states. In this model, the eight states are $[z\ \dot{z}\ q_1\ q_2\ V\ L]$, and the state space model that captures Eqs. 1–11 is given by the following.

$$\begin{aligned}
\dot{x}_1 &= x_2\\
\dot{x}_2 &= \frac{1}{(M+m_\infty)}\Big(-C_{r1}x_3 - C_{r2}x_4 - \rho g A_w(h+x_1)\\
&\qquad -\frac{1}{2}\rho A_w C_d|x_2 - v_f|(x_2 - v_f) + f_{\text{ext}} + f_{\text{PTO}}\Big)\\
\dot{x}_3 &= A_{r1}x_3 + A_{r2}x_4 + A_{r3}x_5 + A_{r4}x_6 + x_2\\
\dot{x}_4 &= x_3\\
\dot{x}_5 &= -k_l\cdot P_a(x_7) - \frac{D}{J}\cdot x_8 + S\cdot x_2\\
\dot{x}_6 &= D\cdot\eta_m\cdot P_a(x_7) - \frac{B}{J}\cdot x_8 - T
\end{aligned} \quad (12)$$

For control, both a linear and nonlinear version of the model will be leveraged. The nonlinear model presented in Eq. 12 will serve as the plant model and also be utilized in the nonlinear MPC strategy. A linearized version of the plant will be used for the linear MPC. For the linear model, the drag force is ignored. The nonlinear terms in Eqs. 8 and 11 are also linearized to provide a simple state space model with the following form for the dynamics of states 2, 5, and 6. Although some forces are small, the linear model will carry with it errors depending on the conditions.

$$\begin{aligned}
\dot{x}_2 &= \frac{1}{(M+m_\infty)}(-C_{r1}x_3 - C_{r2}x_4 - C_{r3}x_5 - C_{r4}x_6\\
&\qquad -\rho g A_w(h+x_1) + f_{\text{ext}} + f_{\text{PTO}})\\
\dot{x}_7 &= -k_l\cdot C_7 - \frac{D}{J}\cdot x_8 + S\cdot x_2\\
\dot{x}_8 &= D\cdot\eta_m\cdot C_8 - \frac{B}{J}\cdot x_8 - T
\end{aligned} \quad (13)$$

Control Framework

Four control frameworks were explored in this work to examine the impact of the control structure and system constraints in each of these paradigms. The first option was considered as the baseline case and leveraged a control that computed the desired PTO force as proportional to the WEC velocity, as illustrated in Fig. 4.

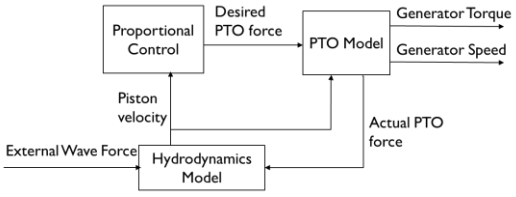

Fig. 4 Base proportional WEC PTO control

Second, a linear MPC was used that leveraged the linear state space model in the MPC but only included the first six states related to the WEC hydrodynamics. As such, the MPC is simpler and should be more computationally efficient, but it has no knowledge of the underlying PTO dynamics. This reduced-state linear MPC aims only to optimize the WEC motion so as to maximize the force entering into the PTO system. The MPC cost function is structured to maximize the WEC velocity within position constraints. The MPC provides a desired PTO force, and the full-state space model is used to compute the actual PTO force achievable and translate this into a final generator torque and speed, as shown in Fig. 5. The nonlinear model is used in the PTO and hydrodynamics model blocks.

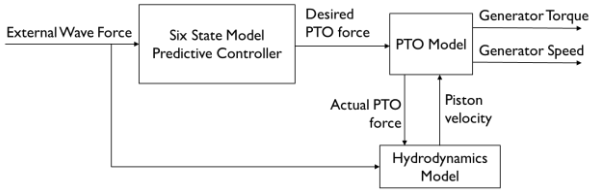

Fig. 5 Reduced-state MPC WEC PTO control

Third, an MPC was integrated, which has full knowledge of the entire system dynamics, including the PTO, but still leverages a linear model. As seen in Fig. 6, the MPC uses the full eight-state model in Eq. 12 but with the simplified linear expressions for states 2, 7, and 8, as shown in Eq. 13. The full-state MPC predicts the torque that the PTO should output. This desired torque command is passed on the underlying PTO system. The PTO model and hydrodynamics model are nonlinear. The MPC cost function is still structured to maximize the WEC velocity but, in this case, has both position and torque constraints integrated. The cost function weighting has been optimized to maximize power output without producing constraint violation.

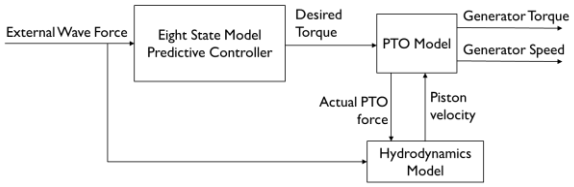

Fig. 6 Full-state MPC WEC PTO control

Finally, a nonlinear MPC was used with the full eight-state model. For this scenario, the same structure is used as in Fig. 6, but the model leveraged for the MPC is the full nonlinear model in Eq. 12.

RESULTS

With the base control strategy, a PTO force is dictated that is proportional to the speed of the WEC. This can easily lead to positions and forces that exceed the systems constraints. The WEC PTO system considered here has a position range of 3.2 m and is modeled after the constraints of the TALOS WEC in which there would be strict limits on the motion of the main mass. In the initial case, only two physical limitations are placed on the system: (1) the accumulator volume must be between zero and the maximum volume, and (2) the generator speed must be positive. As illustrated in Fig. 7a, if no constraints are imposed (shown by the case denoted by "Base"), the WEC position has a range of over 20 m, meaning that in a constrained device, damage would likely occur.

Without constraints, the power production is theoretically high as a result of the high motion, but the inner mass would collide with the outer hull before any useful power could be produced. With constraints (as shown by the case denoted by "Base w/C"), the system operates with larger PTO forces (Fig. 7b) and is able to produce an average power output of 1.9 MW. The position constraint properly restrains motion to an area that avoids collisions. Spectral analysis of the signals illustrates that PTO forces are composed more significantly of low-frequency

(below 1 Hz) and high-frequency (from 19 to 20 Hz) signals. This is in line with the spectrum of the wave excitation force. The accumulator volume and power have frequency components from 0 to 20 Hz, with a more even distribution but slight increases at low and high frequencies.

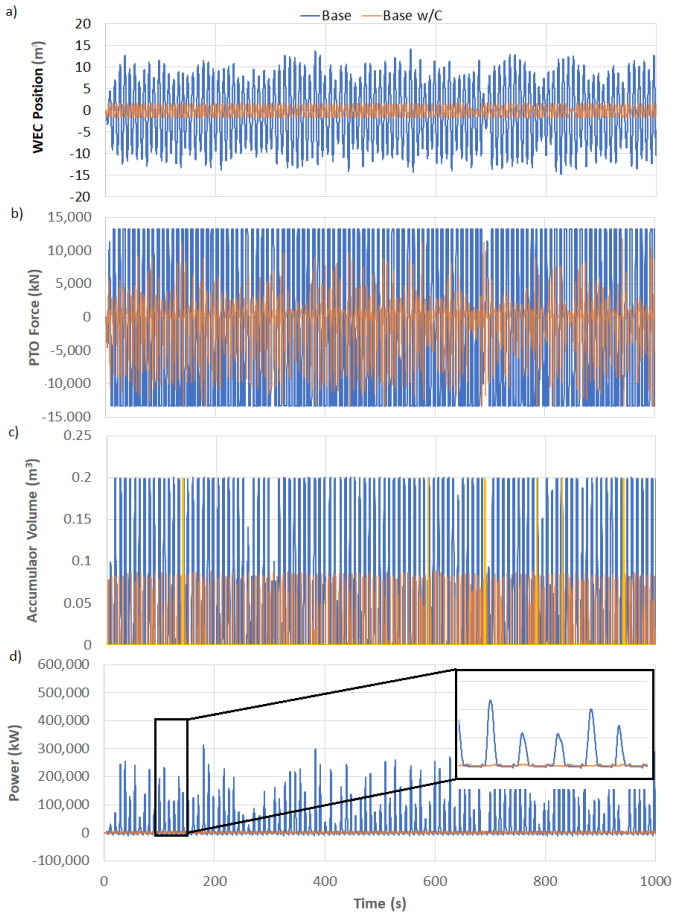

Fig. 7 (a) Wave position, (b) PTO force, (c) accumulator volume, and (d) power for the base control method

The reduced-state linear MPC (RS LMPC) optimizes the power production by seeking to maximize the WEC velocity. Because the six-state version of MPC has no knowledge of the underlying PTO dynamics, it cannot directly maximize the WEC power output. Instead, like the base case, it must choose the PTO force that produces the largest WEC motions and pass this PTO force command off to the PTO system. The PTO control uses a simple feedforward method to calculate the required generator torque needed to produce the desired PTO force based on the dynamics in Eqs. 7 and 9.

Unlike the base case, the MPC can build its decisions on a forecast of the upcoming wave that should, in theory, improve its outcome. In reality, the MPC is unable to properly optimize without at least position constraints. In the case with no constraints, the RS LMPC quickly drives the WEC velocity to infinity, which would lead to damage and failure. Once constrained, the RS LMPC is able to properly optimize and, as illustrated in Fig. 8a, drives the WEC rapidly through its full range of motion in a similar fashion as the base control. PTO forces are lower on average, and the resulting power is higher than the constrained base method but with larger spikes. In this initial case, only a short horizon of five time steps or 0.25 s is assumed. Unlike the base controller, the RS LMPC uses all of the available accumulator volume.

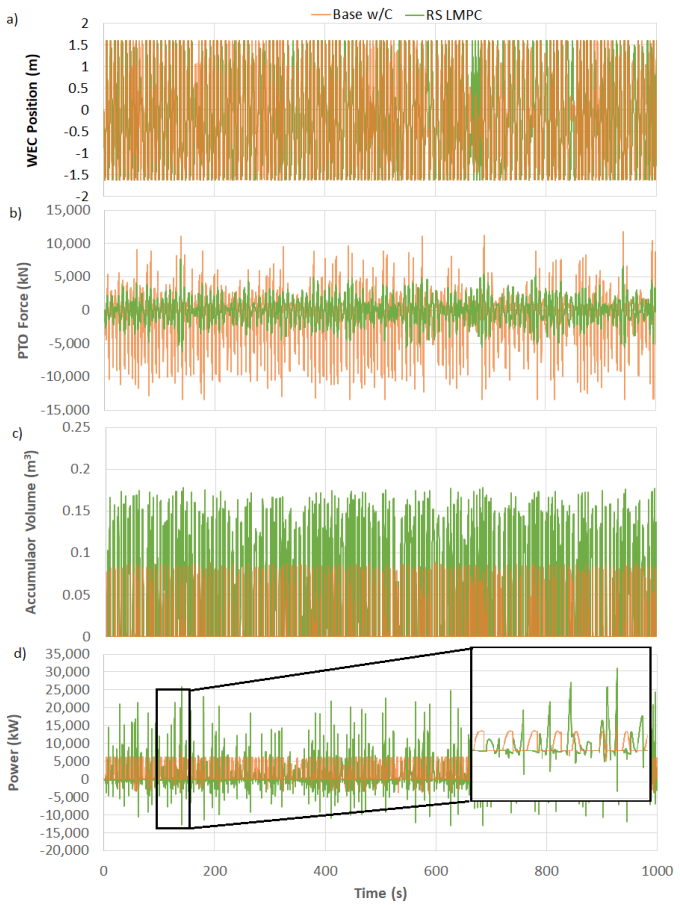

Fig. 8 (a) Wave position, (b) PTO force, (c) accumulator volume, and (d) power for the RS LMPC method

One critical factor for the model predictive control options is the prediction horizon over which it can optimize. A longer prediction horizon should allow the controller to better optimize power production but will come at a higher computational price. The influence of the prediction horizon for the RS LMPC option is shown in Fig. 9. Increasing the prediction horizon improves the power output but only by 67% in the best-case scenario. Extending the prediction horizon beyond 3 s has a detrimental effect, and power production is poor beyond this point. The larger prediction horizon (up to 3 s) improves performance but has a negligible impact in computational speed. By contrast, increasing the control horizon did not have a sizable influence on the power output but increased the computational time and was not examined further.

In contrast to the base and reduced-state linear MPC options, the full-state linear MPC is able to base its control commands on the WEC hydrodynamics as well as the PTO dynamics. It is able to outperform the other methods but requires proper weighting and constraints. Similar to the RS LMPC, it will tend to drive the WEC velocity to infinity if position constraints are not imposed. It is also sensitive to output weighting. If the power output is not sufficiently weighted in the optimization, the system can tend to translate the motion of the mass into hydraulic fluid motion without producing much power as was observed in the base control case without constraints. If the weighting is increased, power output will improve significantly, but if the weight becomes too high, it can drive the PTO force to very high levels. As

such, constraints on position and PTO force are essential with this control option.

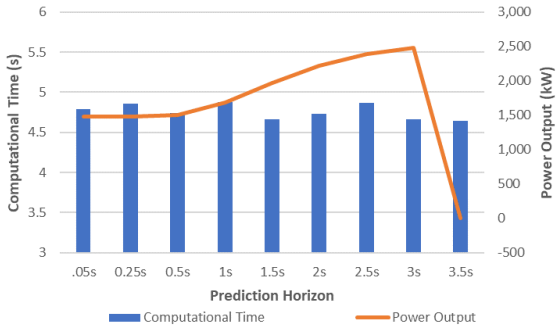

Fig. 9 Impact of prediction horizon on computational time and power output for RS LMPC

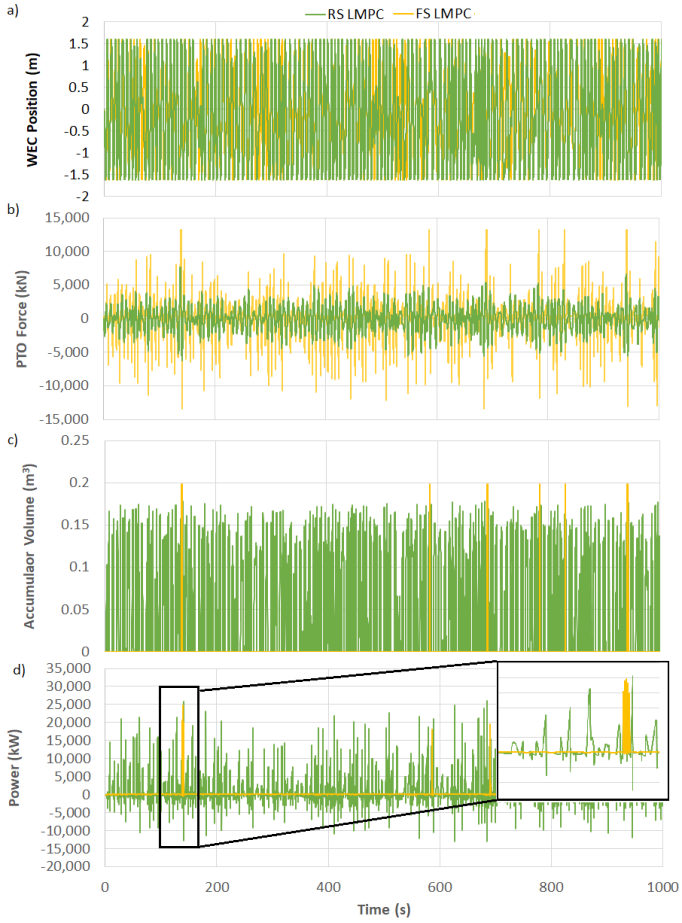

Fig. 10 (a) Wave position, (b) PTO force, (c) accumulator volume, and (d) power for the FS LMPC method

As illustrated in Fig. 10, the full-state linear MPC (FS LMPC) leads to more motion and higher PTO forces. The resulting power output is higher than the reduced-state option because negative power needs are avoided. However, there are also higher power spikes, as seen in the zoomed-in view in Fig. 10d, which could be problematic. Spectral analysis confirms that the power spectrum has more significant peaks although they are distributed from 0 to 5 Hz and 15 to 20 Hz. Additional constraints on the rates of changes in PTO forces or torque commands may be essential to providing smoother, more consistent power output with this control option.

The FS LMPC had a larger increases computational time compared with the RS LMPC case with computational time increasing by 19% when moving from a prediction horizon of 0.25 s to 3 s. Increasing the horizon with the reduced-state option led to a 67% improvement in power output, and with the FS LMPC, a similar increase is seen. With FS LMPC, an increase of 45% is seen in power output when moving from a 0.25 s to 3 s horizon. In both cases, a longer horizon is better, but in the FS LMPC case, the power output improves significantly with a 1.5 s horizon, and only minor improvements are seen at longer horizons. However, these predicted power outputs are higher than realistically achievable because they create some of the high fluctuations such as those observed in the nonlinear MPC case to follow.

Although the FS LMPC provides an improved power output, it is still basing its optimization on the linear model. Improved performance should be feasible if the MPC is able to use the full nonlinear model for its calculation. Figure 11 compares the performance of the full-state nonlinear MPC (FS NLMPC) using the full eight-state nonlinear model with the corresponding linear option. Power output is significantly increased, but this comes at a cost. There is a ~1,000% increase in computational time and much more drastic control actions. The PTO force changes frequently and is driven from the maximum achievable to the minimum, which in turn drives rapid fluctuations in the accumulator from its maximum volume all the way to zero volume. Spectral analysis confirms that the power and accumulator volume

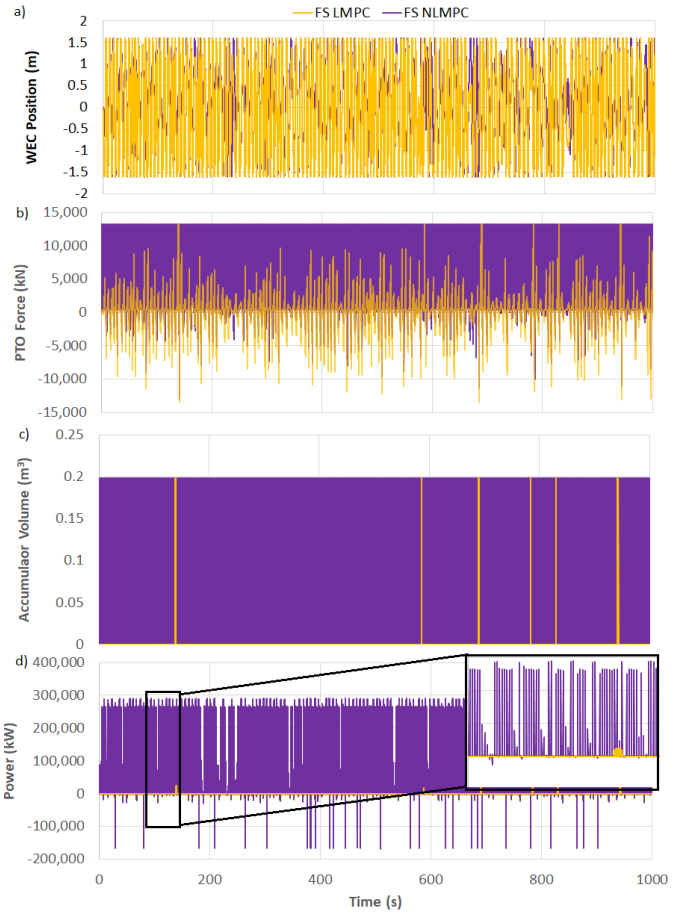

Fig. 11 (a) Wave position, (b) PTO force, (c) accumulator volume, and (d) power for the eight-state nonlinear MPC method

spectrum has more significant peaks, but frequencies from 0 to 20 Hz

are more evenly represented in the signal. This control option is also a very sensitive to weightings. Although the computational time is likely not excessive enough to cause a large limitation for the simple 1D case, limitations may be encountered in the multi-degree-of-freedom system. In addition, the high sensitivity of this controller and its tendency to potentially overactuate the system could limit its utility. This control approach, such as the FS LMPC option, would likely need additional constraints on the rates of change of the PTO force and torque to avoid unrealistic fluctuations.

In all four control cases considered, constraints on position are essential. Without position constraints, the base control produces a fairly immediate collision between the hull and central mass. In other words, the combination of overly simple control without limitations leads an unfunctional WEC system. Although this could be anticipated, these results illustrate the magnitude that these differences can make in the power output. Once constraints are in place, the base control is able to produce an average power output of 1.9 MW.

Constraints are even more critical with MPC. Because MPC seeks to optimize power output, it can send the velocity to infinity. As such, MPC needs position or velocity constraints to function. All the reduced-state and full-state MPC options considered have this need for constraints. Once constraints are imposed, all MPC options work and perform better than the base control option. The reduced-state linear version is only able to base its optimization on the linear hydrodynamics of the WEC and is able to achieve an average power output of 2.5 MW, a 31% improvement over that of the base option.

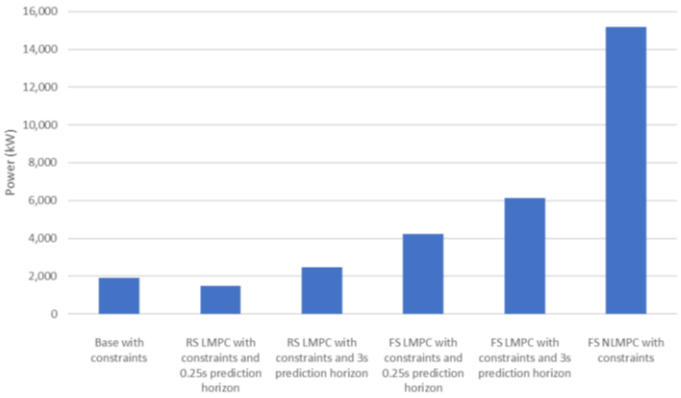

Fig. 12 Comparison of average power output for the various control cases considered

The FS LMPC provides a further improvement as the controller is able to better account for the PTO dynamics to some degree in its optimization. The FS LMPC produces 4.2 MW with a shorter horizon and 6.1 MW with a longer prediction horizon, up to a 148% improvement over the six-state option and a 224% improvement from the base control. The base control and linear MPC options are all outperformed by the nonlinear MPC, which theoretically produces over 15 MW of power output. However, the nonlinear case creates rapid fluctuations that would be problematic in real life. It tends to order discrete changes to the system that result in sudden changes in hydraulic motor speed and torque and rapid filling and emptying of the accumulator. If the rate of changes of these actuations is limited, the performance will become closer to that of the linear MPC, but further exploration of this will be pursued in future work. Figure 12 compares the average power output of each control option.

CONCLUSIONS AND FUTURE WORK

This work explored a simple proportional PTO control and three different control structures that leverage MPC. The results demonstrate that if the system constraints are ignored, extremely poor performance is achieved regardless of control strategy. Providing the MPC with more information on which to base its optimization enables improvements in the power output. However, constraints are essential to proper power production. Without position or velocity constraints, the MPC will not be able to provide realistic solutions. Further constraints on the PTO force and torque output are also needed to avoid the MPC attempting to ask for forces beyond the physical constraints of the system. Leveraging a nonlinear model in the MPC can improve power production, but the tendency of this control strategy to overreact may provide practical limitations on the utility of the approach. Although there is much more to be explored in this area, this study provides an idea of the relative effectiveness of these control approaches. Future work will examine the utility of frequency limits into the MPC to limit sudden actuator changes and will explore the extension of these control methods to the three-dimensional case of the TALOS WEC design. Experimental testing of the TALOS control design will also be conducted in the future.

ACKNOWLEDGEMENTS

This work was partially supported by the US-UK Fulbright Commission through the Fulbright-Lancaster University Scholar Award 2022–2023. Additional funding was provided by the UK Engineering and Physical Sciences Research Council (EPSRC Grant No. EP/V040561/1) for the project Novel High-Performance Wave Energy Converters (NHP-WEC) with advanced control, reliability, and survivability systems through machine-learning forecasting. W. Sheng's current affiliation is South East Technological University, Carlow, Ireland.

REFERENCES

Aderinto, T, and Li, H (2018). "Ocean Wave Energy Converters: Status and Challenges," *Energies*, 11(5), 1250.

Aggidis, G, and Taylor, C (2017). "Overview of Wave Energy Converter Devices and the Development of a New Multi-axis Laboratory Prototype," *IFAC-PapersOnLine*, 50(1), 15651–15656.

Amann, KU, Magaña, ME, and Sawodny, O (2014). "Model Predictive Control of a Nonlinear 2-Body Point Absorber Wave Energy Converter with Estimated State Feedback," *IEEE Trans Sustainable Energy*, 6(2), 336–345.

Bacelli, G, Genest, R, and Ringwood, J (2015). "Nonlinear Control of Flap-type Wave Energy Converter with a Non-ideal Power Take-off System," *Annu Rev Control*, 40, 116–126.

Bacelli, G, Gilloteaux, J-C, and Ringwood, J (2008). "State Space Model of a Hydraulic Power Take off Unit for Wave Energy Conversion Employing Bondgraphs," *Proc World Renewable Energy Congr*, Glasgow, Scotland, WREC, 01.

Bacelli, G, and Ringwood, JV (2013). "A Geometric Tool for the Analysis of Position and Force Constraints in Wave Energy Converters," *Ocean Eng*, 65, 10–18.

Bracco, G, Canale, M, and Cerone, V (2020). "Optimizing Energy Production of an Inertial Sea Wave Energy Converter via Model Predictive Control," *Control Eng Pract*, 96, 104299.

Brekken, TK (2011). "On Model Predictive Control for a Point Absorber Wave Energy Converter," *2011 IEEE Trondheim PowerTech*, Trondheim, Norway, IEEE, 1–8.

Brown, A, Thomson, J, and Rusch, C (2017). "Hydrodynamic Coefficients of Heave Plates, with Application to Wave Energy Conversion," *IEEE J Oceanic Eng*, 43(4), 983–996.

Cavaglieri, D, Bewley, TR, and Previsic, M (2015). "Model Predictive

Control Leveraging Ensemble Kalman Forecasting for Optimal Power Take-off in Wave Energy Conversion Systems," *2015 Am Control Conf*, Chicago, IL, USA, IEEE, 5224–5230.

Duarte, T, Sarmento, A, Alves, M, and Jonkman, J (2013). *State-space Realization of the Wave-radiation Force within FAST*, Preprint, National Renewable Energy Lab, 12 pp.

Faedo, N, Olaya, S and Ringwood, JV (2017). "Optimal Control, MPC and MPC-like Algorithms for Wave Energy Systems: An Overview," *IFAC J Syst Control*, 1, 37–56.

Faedo, N, Scarciotti, G, Astolfi, A, and Ringwood, JV (2018). "Energy-maximising Control of Wave Energy Converters Using a Moment-domain Representation," *Control Eng Practice*, 81, 85–96.

Fusco, F, and Ringwood, JV (2013). "A Simple and Effective Real-time Controller for Wave Energy Converters," *IEEE Trans Sustainable Energy*, 4(1), 21–30.

Garcia-Rosa, PB, Lizarralde, F, and Estefen, SF (2012). "Optimization of the Wave Energy Absorption in Oscillating-body Systems Using Extremum Seeking Approach," *2012 Am Control Conf*, Montreal, QC, Canada, IEEE, 1011–1016.

García-Violini, D, Faedo, N, Jaramillo-Lopez, F, and Ringwood, JV (2020). "Simple Controllers for Wave Energy Devices Compared," *J Mar Sci Eng*, 8(10), 793.

Garcia-Violini, D, and Ringwood, JV (2021). "Energy Maximising Robust Control for Spectral and Pseudospectral Methods with Application to Wave Energy Systems," *Int J Control*, 94(4), 1102–1113.

Genest, R, and Ringwood, JV (2016). "Receding Horizon Pseudospectral Control for Energy Maximization with Application to Wave Energy Devices," *IEEE Trans Control Syst Technol*, 25(1), 29–38.

Haider, AS, Brekken, TK and McCall, A (2021). "Real-time Nonlinear Model Predictive Controller for Multiple Degrees of Freedom Wave Energy Converters with Non-ideal Power Take-off," *J Mar Sci Eng*, 9(8).

Hals, J, Falnes, J, and Moan, T (2011a). "A Comparison of Selected Strategies for Adaptive Control of Wave Energy Converters," *J Offshore Mech Arct Eng*, 133(3), 031101.

Hals, J, Falnes, J, and Moan, T (2011b). "Constrained Optimal Control of a Heaving Buoy Wave-energy Converter," *J Offshore Mech Arct Eng*, 133(1), 011401.

Hendrikx, RWM, Leth, J, Andersen, P, and Heemels, WPMH (2017). "Optimal Control of a Wave Energy Converter," *2017 IEEE Conf Control Technol Appl*, Maui, HI, USA, IEEE, 779–786.

Jama, M, and Wahyudie, A (2017). "Online Damping Strategy for Controlling Heaving Wave Energy Converters Using Three-phase Bridge Boost Rectifier," *IEEE Access*, 5, 7682–7691.

Jama, M, Wahyudie, A, Assi, A, and Noura, H (2014). "Function-based Model Predictive Control Approach for Maximum Power Capture of Heaving Wave Energy Converters," *ICREGA'14-Renewable Energy Gener Appl*, Springer, 299–313.

Karthikeyan, A, Previsic, M, Scruggs, J, and Chertok, A (2019). "Non-linear Model Predictive Control of Wave Energy Converters with Realistic Power Take-off Configurations and Loss Model," *2019 IEEE Conf Control Technol Appl*, Hong Kong, China, IEEE, 270–277.

Kovaltchouk, T, Rongère, F, Primot, M, Aubry, J, Ahmed, HB, and Multon, B (2015). "Model Predictive Control of a Direct Wave Energy Converter Constrained by the Electrical Chain Using an Energetic Approach," *Eur Wave Tidal Energy Conf*, Nantes, France.

Li, G (2017). "Nonlinear Model Predictive Control of a Wave Energy Converter Based on Differential Flatness Parameterization," *Int J Control*, 90(1), 68–77.

Li, G, and Belmont, MR (2014). "Model Predictive Control of Sea Wave Energy Converters Part I: A Convex Approach for the Case of a Single Device," *Renewable Energy*, 69, 453–463.

Mérigaud, A, and Tona, P (2020). "Spectral Control of Wave Energy Converters with Non-ideal Power Take-off Systems," *J Mar Sci Eng*, 8(11), 851.

O'Sullivan, AC, and Lightbody, G (2017). "Co-design of a Wave Energy Converter Using Constrained Predictive Control," *Renewable Energy*, 102, 142–156.

Parker, RPM, Harrison, G, and Chick, J (2007). "Energy and Carbon Audit of an Offshore Wave Energy Converter," *Proc Inst Mech Eng Part A J Power Energy*, 221(8), 1119–1130.

Pasta, E, Faedo, N, Parrinello, L, Carapellese, F, Ringwood, JV, and Mattiazzo, G (2021). "Constraint Handling in Extremum-seeking Control for Wave Energy Systems: A Case Study," *2021 Int Conf Electr Comput Commun Mechatron Eng*, Mauritius, Mauritius, IEEE, 1–6.

Penalba, M, and Ringwood, JV (2019). "Linearisation-based Nonlinearity Measures for Wave-to-wire Models in Wave Energy," *Ocean Eng*, 171, 496–504.

Previsic, M, Karthikeyan, A, and Scruggs, J (2021). "A Comparative Study of Model Predictive Control and Optimal Causal Control for Heaving Point Absorbers," *J Mar Sci Eng*, 9(8), 805.

Quartier, N, Ropero-Giralda, P, Domínguez, JM, Stratigaki, V, and Troch, P (2021). "Influence of the Drag Force on the Average Absorbed Power of Heaving Wave Energy Converters Using Smoothed Particle Hydrodynamics," *Water*, 13(3), 384.

Richter, M, Magaña, ME, Sawodny, O, and Brekken, TK (2014). "Power Optimisation of a Point Absorber Wave Energy Converter by Means of Linear Model Predictive Control," *IET Renewable Power Gener*, 8(2), 203–215.

Ringwood, JV (2020). "Wave Energy Control: Status and Perspectives 2020," *IFAC-PapersOnLine*, 53(2), 12271–12282.

Sergiienko, NY, Bacelli, G, Coe, RG, and Cazzolato, BS (2022). "A Comparison of Efficiency-aware Model-predictive Control Approaches for Wave Energy Devices," *J Ocean Eng Mar Energy*, 8(1), 17–29.

Sergiienko, NY, Cocho, M, Cazzolato, BS, and Pichard, A (2021). "Effect of a Model Predictive Control on the Design of a Power Take-off System for Wave Energy Converters," *Appl Ocean Res*, 115, 102836.

Sheng, W, Tapoglou, E, Ma, X, Taylor, CJ, Dorrell, R, Parsons, DR, and Aggidis, G (2022). "Time-domain Implementation and Analyses of Multi-motion Modes of Floating Structures," *J Mar Sci Eng*, 10(5), 662.

Sun, Z, Zhao, A, Zhu, L, Lu, K, Wu, W, and Blaabjerg, F (2018). "Extremum-seeking Control of Wave Energy Converters Using Two-objective Flower Pollination Algorithm," *2018 IEEE Int Power Electron Appl Conf Exposition*, Shenzhen, China, IEEE, 1–5.

Têtu, A (2017). "Power Take-off Systems for WECs," In *Handbook of Ocean Wave Energy*, Pecher, A, and Kofoed, JP (Eds), Springer International Publishing, 203–220.

Windt, C, Faedo, N, Penalba, M, Dias, F, and Ringwood, JV (2021). "Reactive Control of Wave Energy Devices—The Modelling Paradox," *Appl Ocean Res*, 109, 102574.

Zhan, S, Na, J, Li, G, and Wang, B (2020). "Adaptive Model Predictive Control of Wave Energy Converters," *IEEE Trans Sustainable Energy*, 11(1), 229–238.

Zhang, Y, and Li, G (2022). "Robust Tube-based MPC for Wave Energy Converters," *IEEE Trans Sustainable Energy*, 1–9.